A Method for Incorporating Frequency Nadir Limits in Power System Restoration Planning

Xiangyu Zou
ECE Department
University of Toronto
Toronto, ON, Canada
xy.zou@mail.utoronto.ca

Ilyas Farhat
ECE Department
University of Toronto
Toronto, ON, Canada
ilyas.farhat@utoronto.ca

John W. Simpson-Porco
ECE Department
University of Toronto
Toronto, ON, Canada
jw.simpson@utoronto.ca

***Abstract*—Power system restoration following a black out involves a sequence of actions to recover the network. Restoration planning must be aware of the dynamic impacts of each restorative action and ensure that they do not compromise the system's security. In this work, we construct a frequency-constrained mixed-integer linear (MILP) to find fast and dynamically secure restoration plans. We present a novel frequency nadir prediction method that uses the unique knowledge of the magnitude and timing of electrical disturbances during restoration. The predictions are used to introduce frequency nadir constraints, which are linearized through a receding-horizon solution approach to the MILP. A case study simulated in MATLAB and PSS/E illustrates the effectiveness of the proposed frequency prediction and optimization methods.**

***Index Terms*—Power System Restoration, Frequency Nadir Estimation, Mixed-Integer Programming**

I. Introduction

Widespread power outages impose significant financial burdens, impact critical infrastructure, and result in economic losses of up to billions of dollars per incident [1]. Historical evidence shows that proactive planning and rapid restoration efforts can significantly alleviate these impacts, reducing total economic damages by up to 96% in prolonged outages [1]. In traditional restoration practices, Independent System Operators (ISOs) designate several Synchronous Generators (SGs)—often hydro or gas turbine generators—as Black-Start Units (BSUs), which can self-start without external power. These units supply initial power to energize transmission lines, start Non-Black-Start Units (NBSUs), and restore loads [2]–[5].

During restoration, the system must withstand dynamic frequency effects from sequential actions, a growing concern in reduced-inertia systems with inverter-based resources (IBRs) and distributed energy resources (DERs) [6]–[8]. To prevent large frequency drops that exceed safe thresholds (e.g. 59.5 Hz) and cause under-frequency load shedding, operators impose conservative rules on load pickup, e.g., limiting it to no more than 5% of online generation [2]–[5], [9]. While these rules are designed to ensure system stability, they may overly limit the speed of load pickups and delay system recovery. To reduce restoration time without compromising reliability, the frequency impacts of restorative actions must be considered during the planning process.

Related Work: The IEEE task force reports [3], [4] present foundational concepts for restoring generation, reconfiguring transmission and incrementally picking up loads; however, their main focus is on voltage and reactive power security. Restoration approaches for distribution systems, including [7], [10], emphasize structural recovery and feeder reconfiguration, but do not explicitly address frequency-related constraints. A heuristic recursive algorithm to compute restoration plans for transmission lines is presented in [11] as a faster alternative to computationally heavy optimization programs. The work in [8] highlights opportunities for wind participation in the early restoration stages, leveraging probabilistic constraints to accommodate wind power variability. The restoration problem is presented as a nonlinear system driven by feedback control in [12], which allows for the use of real-time measurements. The work in [13] incorporates transient stability into restoration planning by refining generator set points to maintain synchronism, but focuses primarily on line and load recovery and relies on a separate optimization step to address dynamics. Related efforts to model frequency response include [14], which fits parabolic curves to estimate frequency nadirs after disturbances, and [9], which applies parametric fitting to simplify aggregate dynamics of SGs and renewables.

The aforementioned works consider various aspects of restoration, including distribution networks, line energization, NBSU startup properties, and renewable generation. To the best of our knowledge however, no computationally tractable approaches to frequency-constrained restoration planning can be found in the literature.

Contributions: Here we develop and validate a novel method for incorporating frequency nadir constraints into optimal black-start restoration planning. First, based on the large load pick-ups and generation set-point changes that occur during restoration, we develop a novel approximation of the IEEEG1 turbine-governor model, and leverage this approximation to obtain a closed-form bound on the allowable load pick-up for a given frequency nadir limit. The bound is integrated into a mixed-integer linear program (MILP) for black-start restoration planning. As the nadir limit constraint is non-linear in the decision variables (generator statuses),

Research supported by Hydro One Networks Inc. and NSERC ALLRP 597475-2024 "Planning Restoration of Inverter-Based Grids".

we introduce a receding-horizon methodology for computing the restoration plan via a sequence of MILPs. The approach produces secure black-start restoration plans that respect the nadir constraints while quickly restoring load. The approach is validated via a case study on a modified IEEE 9-bus system in both MATLAB and PSS/E.

II. Review: MILP Model for Power System Restoration Planning

We first develop an MILP to compute black-start restoration sequences for transmission systems; the treatment is based largely on the framework proposed in [8]. This section introduces the power flow model, the NBSU start-up model, network logic constraints, and the objective function.

Binary variables are used to model the on and off statuses of network elements. We consider a power system with B buses, L lines, D loads (demands), and G generators, and let $\boldsymbol{b}_{\mathrm{b}} \in \{0,1\}^{B\times T}$, $\boldsymbol{b}_{\mathrm{l}} \in \{0,1\}^{L\times T}$, $\boldsymbol{b}_{\mathrm{d}} \in \{0,1\}^{D\times T}$, $\boldsymbol{b}_{\mathrm{g}} \in \{0,1\}^{G\times T}$ denote matrices of binary variables that indicate the on/off status of the respective components over T discrete time steps. Accordingly, let $\boldsymbol{b}_{\mathrm{b}}^0$, $\boldsymbol{b}_{\mathrm{l}}^0$, $\boldsymbol{b}_{\mathrm{d}}^0$, and $\boldsymbol{b}_{\mathrm{g}}^0$ be column vectors that denote the initial values of the respective variables prior to restoration. In a black-start scenario, only the BSU and the bus it resides on are initially active, and we impose that network elements cannot be turned off once restored.

Let $\boldsymbol{P}_{\mathrm{g}} \in \mathbb{R}^{G\times T}$ and $\boldsymbol{P}_{l} \in \mathbb{R}^{L\times T}$ denote the generator power outputs and network line flows over $\{1,\dots,T\}$ time steps, respectively, and let $\boldsymbol{P}_{\mathrm{d}} \in \mathbb{R}^{D}$ be a vector of load magnitudes. We use the adjacency matrices $\mathbf{A}_{\mathrm{g}} \in \{0,1\}^{B\times G}$ and $\mathbf{A}_{\mathrm{d}} \in \{0,1\}^{B\times D}$ to map network elements to their buses, each defined element-wise as

$$\mathbf{A}_{n,ij} = \begin{cases} 1 & j\text{th element of } n \text{ is connected to bus } i \\ 0 & \text{otherwise.} \end{cases}$$

With this notation, the vectorized real power balance equation at every bus and every time can be compactly written as

$$\mathbf{A}_{\mathrm{g}}\boldsymbol{P}_{\mathrm{g}} - \mathbf{A}_{\mathrm{d}}\,\mathrm{diag}(\boldsymbol{P}_{\mathrm{d}})\boldsymbol{b}_{\mathrm{d}} = \mathbf{A}\boldsymbol{P}_{\mathrm{l}} \tag{1}$$

where $\mathbf{A} \in \mathbb{R}^{B\times L}$ is the network incidence matrix [15]. Power flow on the network is modeled via the DC power flow approximation: all lines are purely reactive, all voltage magnitudes are approximately 1 per unit, and all phase differences between adjacent buses are small [16]. The DC power flow is applied to energized lines, while inactive lines have zero flow. To impose this condition through linear constraints, we adopt the big-M method as in [8], and write the element-wise conditions

$$-M(\mathbb{1} - \boldsymbol{b}_{\mathrm{l}}) \le \boldsymbol{P}_{\mathrm{l}} - \mathbf{X}^{-1}\mathbf{A}^{\top}\boldsymbol{\theta} \le M(\mathbb{1} - \boldsymbol{b}_{\mathrm{l}}) \tag{2a}$$

$$-M\boldsymbol{b}_{\mathrm{l}} \le \boldsymbol{P}_{\mathrm{l}} \le M\boldsymbol{b}_{\mathrm{l}} \tag{2b}$$

where M is a large constant, $\mathbb{1}$ is a matrix of all 1s, $\mathbf{X} \in \mathbb{R}^{L\times L}$ is the diagonal matrix of line reactances, and $\boldsymbol{\theta} \in \mathbb{R}^{B\times T}$ contain bus phases for all time steps. Inequality (2a) handles energized lines, while (2b) handles those that are off.

The start-up procedure of NBSUs can be described by the four phases shown in Fig. 1, which are referred to as the offline (I), cranking (II), ramping (III), and online (IV) phases respectively [17]. During the cranking phase, NBSUs draw fixed power $\boldsymbol{P}_{\mathrm{c}}$ over a period $\boldsymbol{T}_{\mathrm{c}}$; subsequently, they transition to a ramping phase, increasing power output *linearly* at a rate $\boldsymbol{r}$ over a period $\boldsymbol{T}_{\mathrm{r}}$ up to their minimum capacities $\underline{\boldsymbol{P}}_{\mathrm{g}}$. These startup parameters are all column vectors of size $\mathbb{R}^{G}$.

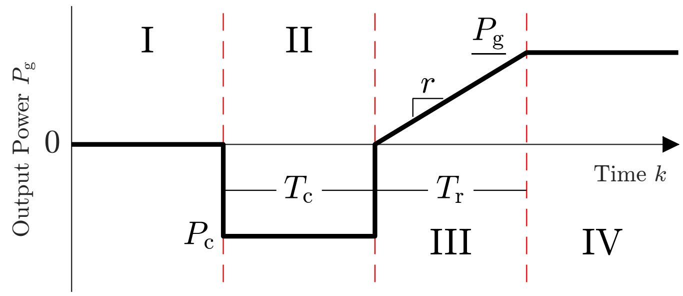

Fig. 1: Start-up behaviour of a NBSU

TABLE I: Logic Table of the NBSU Start-Up Phases

$b_{\mathrm{g}}(k)$	$b_{\mathrm{gc}}(k)$	$b_{\mathrm{gr}}(k)$	$b_{\mathrm{go}}(k)$	$P_{\mathrm{g}}(k)$
0	0	0	0	$P_{\mathrm{g}}(k) = 0$
1	1	0	0	$P_{\mathrm{g}}(k) = -P_{\mathrm{c}}$
1	0	1	0	$P_{\mathrm{g}}(k) = P_{\mathrm{r}}(k)$
1	0	0	1	$\underline{P_{\mathrm{g}}} \le P_{\mathrm{g}}(k) \le \overline{P_{\mathrm{g}}}$
for all $k \in \{1,\dots,T\}$, All other combinations impossible				

Once they are online, generators may operate between their maximum and minimum limits $\underline{\boldsymbol{P}}_{\mathrm{g}}$ and $\overline{\boldsymbol{P}}_{\mathrm{g}}$ while being limited by their ramp rates r. This piecewise behaviour can be expressed via linear constraints using auxiliary binary variables $\boldsymbol{b}_{\mathrm{gc}}, \boldsymbol{b}_{\mathrm{gr}}, \boldsymbol{b}_{\mathrm{go}} \in \mathbb{R}^{G\times T}$, which indicate when the generator is cranking, ramping, or online respectively. Since the duration of the cranking and ramping phases are known, these auxiliary variables are in fact uniquely determined by when generators turn on, i.e., by $\boldsymbol{b}_{\mathrm{g}}$. The desired start-up behaviour for any single NBSU is shown in Table I, where $\boldsymbol{P}_{\mathrm{r}} \in \mathbb{R}^{G\times T}$ is a reference that linearly increases at rate r following the cranking phase. In Table I and going forward, we use the notation $x(k)$ to denote column k of variable x, representing values at the kth time step. Similar to (2), the piecewise-linear behaviour of $\boldsymbol{P}_{\mathrm{g}}$ in Table I can be represented by linear inequalities.

Additional network logic constraints are required to couple the binary status variables. In particular, lines may be energized only if an adjacent bus has been restored. Loads and generators may be restored only if their buses are active. Details are omitted due to space limitations; see [18].

The objective function z to be maximized is

$$z = \sum_{k=1}^{T} \left[\boldsymbol{b}_{\mathrm{g}}(k)^{\top}\boldsymbol{w}_{\mathrm{g}} + \boldsymbol{b}_{\mathrm{d}}(k)^{\top}\mathrm{diag}(\boldsymbol{P}_{\mathrm{d}})\boldsymbol{w}_{\mathrm{d}} + \boldsymbol{b}_{\mathrm{l}}(k)^{\top}\boldsymbol{w}_{\mathrm{l}}\right]$$

where $\boldsymbol{w}_{\mathrm{g}} \in \mathbb{R}^{G}$, $\boldsymbol{w}_{\mathrm{d}} \in \mathbb{R}^{D}$, $\boldsymbol{w}_{\mathrm{l}} \in \mathbb{R}^{L}$ are weight vectors that specify the degree of importance given to each generator, load, and line. This allows certain loads, such as critical infrastructure, to be prioritized. To guide weight selection, restoration sequences should first prioritize NBSU start-ups for the additional power capacity and stabilizing inertia they provide [2]. As restoration progresses, more power becomes available to energize the remaining lines and loads. Following these goals, the weights should be chosen such that $\boldsymbol{w}_{\mathrm{g}} \gg \boldsymbol{w}_{\mathrm{d}} \gg \boldsymbol{w}_{\mathrm{l}}$. This encourages quickly starting the NBSUs and shifts the focus to loads once all generators are activated.

In brief notation, and where some mathematical expressions are omitted due to space limitations, the complete restoration framework can be expressed as

$$\begin{aligned} &\text{maximize} \quad z \\ &\text{subject to} \quad \text{Power balance (1), Line flows (2a) (2b)} \\ &\qquad\qquad\quad \text{NBSU Startup, Network Logic} \end{aligned} \tag{3}$$

Our next goal is the integration of dynamic frequency constraints into the baseline restoration planning problem (3).

III. Frequency Nadir Computation via Ramp-Approximated Governor Model

A. Primary Frequency Response Model

During restoration, frequency must be maintained around its nominal value to ensure operational security. We consider primary frequency response (PFR) from BSUs, with optional contributions from selected NBSUs, to maintain frequency stability as new loads are incrementally energized. We are interested in quantifying the *frequency nadir*, i.e., the lowest frequency reached following a step electrical disturbance. To prevent triggering under-frequency protection systems and damaging network elements, the nadir must not deviate from the nominal by more than a safe threshold $|\Delta\omega_{\mathrm{lim}}|$ to be defined by the system operator.

We consider an Average System Frequency (ASF) model, which captures the system-wide frequency dynamics using an aggregated inertia and individual turbine-governor models for each SG [19].[1] The ASF dynamics are governed by the swing equation

$$\Delta\dot{\omega}(t) = \frac{1}{2H_{\mathrm{sys}}}\left(\sum\nolimits_{i=1}^{G} \alpha_i \Delta P_{\mathrm{m}}^{i}(t) - \Delta P_{\mathrm{e}}(t)\right), \tag{4}$$

which relates power imbalance to the rate of frequency change, where $\Delta\omega(t)$ is the per unit frequency deviation, H_{sys} is the lumped system inertia, $\Delta P_{\mathrm{m}}^{i}$ is the mechanical power of the ith turbine, α_i converts units from the machine base to the system base, and ΔP_{e} is the electrical power imbalance. We assume that ΔP_{e} takes positive values, which represents step power shortages from load and generator pickup. The model (4) holds *between* each discrete restoration step.

During restoration, generators (i) contribute to system inertia at the start of their ramping phase, when they become synchronized, and (ii) contribute to primary frequency response once they are online. *Thus the inertia H_{sys} and conversion factors α_i in (4) vary with the discrete restoration time step $k \in \{1, \ldots, T\}$ over the horizon T.* Denoting by $\boldsymbol{H}_{\mathrm{sys}} \in \mathbb{R}^{1\times T}$ the time-vector of inertia, we have the relationship

[1] For systems incorporating IBRs, the Generic System Frequency Response (G-SFR) model from [9] can alternatively be used.

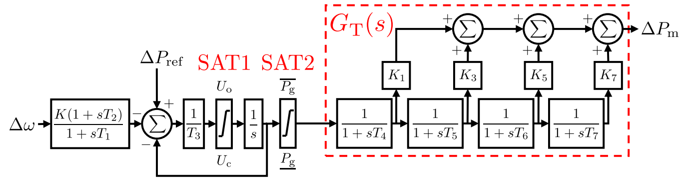

Fig. 2: IEEEG1 governor turbine model

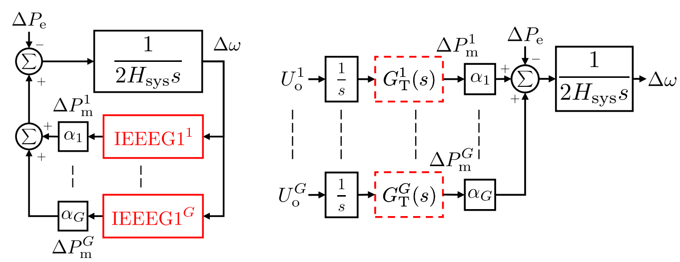

(a) (b)

Fig. 3: (a) Closed-loop ASF model; (b) Broken feedback loop using the ramp approximation.

$$\boldsymbol{H}_{\mathrm{sys}}(k) = \tfrac{1}{S_{\mathrm{sys}}} \overline{\boldsymbol{P}}_{\mathrm{g}}^{\top} \operatorname{diag}(\boldsymbol{H})(\boldsymbol{b}_{\mathrm{gr}}(k) + \boldsymbol{b}_{\mathrm{go}}(k)) \tag{5}$$

for all $k \in \{1, \ldots, T\}$, where $\boldsymbol{b}_{\mathrm{gr}}$ and $\boldsymbol{b}_{\mathrm{go}}$ are the previously defined binary variables for ramping and online generators, $\boldsymbol{H} \in \mathbb{R}^{G}$ is a vector that contains inertia constants of individual generators, and S_{sys} is the system base. Similarly, letting $\boldsymbol{\alpha} \in \mathbb{R}^{G\times T}$ denote the matrix of unit conversion factors, we have the relationship

$$\boldsymbol{\alpha}(k) = \tfrac{1}{S_{\mathrm{sys}}} \operatorname{diag}(\overline{\boldsymbol{P}}_{\mathrm{g}})\boldsymbol{b}_{\mathrm{go}}(k), \qquad k \in \{1, \ldots, T\}. \tag{6}$$

In what follows, we examine the frequency dynamics at an arbitrary restoration time step, and assume that frequency is restored to its nominal value before the next restoration action is taken. This is achieved by secondary frequency control, a slower control process on the timescale of minutes, which can therefore be neglected for the purposes of nadir prediction. For notational simplicity, we use the unbolded variables $H_{\mathrm{sys}} \in \mathbb{R}$ and $\alpha \in \mathbb{R}^{G}$ to indicate their values at any single time step.

B. IEEEG1 Model and Ramp Approximation

We adopt the IEEEG1 turbine-governor model [20], shown in Fig. 2. The model features two saturator blocks: SAT1, which limits the output power rate of change, and SAT2, which limits the output power magnitude. We neglect SAT2 by assuming that a sufficient dynamic reserve is allocated such that generators assigned with delivering PFR do not reach their maximum capacities. The block diagram of the swing equation (4) with the turbine-governors is shown in Fig. 3a. Our goal is to obtain an approximate formula for the frequency nadir that occurs due to a load pick-up during restoration.

During normal operating conditions, the set-points P_{ref} to the governors remain unchanged, and all PFR response occurs through the frequency feedback loop. However, since power imbalances introduced by restorative actions have known magnitude and timing, generator set points can be actively adjusted simultaneously during restoration to improve the speed of PFR. In Fig. 2, a positive ΔP_{ref} will accelerate the governor response by feeding an initial value $\frac{\Delta P_{\mathrm{ref}}}{T_3}$ to SAT1. A natural way to update the set points for each responding unit to adjust its set point by the common per-unit amount

$$\Delta P_{\mathrm{ref}} = \frac{\Delta P_{\mathrm{e}}}{\sum_{i=1}^{G} \alpha_i}. \tag{7}$$

By sending the same per-unit set point to each generator, each generator will contribute to the frequency response proportional to its capacity, and the sum of the set point changes following unit adjustment is equal to the load magnitude ΔP_{e}.

Note that for large disturbances, the initial value entering SAT1, $\frac{\Delta P_{\mathrm{ref}}}{T_3}$, where T_3 is a small time constant, will exceed the upper saturation limit U_{o}. The value entering SAT1 will continue to rise as the system frequency declines from the imbalance, and will decrease as frequency is restored. Importantly, this means that SAT1 will unsaturate *only after the nadir is reached*. Therefore, to estimate the frequency nadir, we may assume that the SAT1 output has a constant value of U_{o}, resulting in the simplified block diagram in Fig. 3b where $G_{\mathrm{T}}(s)$ denote the turbine models from Fig. 2

We term the broken feedback system in Fig. 3b the *ramp approximation model*. Under this assumption, all responding generators increase their power output at a maximum rate upon detecting a power imbalance. The approximation accuracy improves with larger disturbances that cause lower frequency nadirs, a fact which is aligned with the goal of finding the maximum permissible imbalance for a given frequency nadir limit. In this model, the mechanical power of any machine is the turbine response to a linear ramp with slope U_{o}, given in the Laplace domain by

$$\Delta P_{\mathrm{m}}^{i}(s) = \frac{U_{\mathrm{o}}^{i}}{s^2} G_{\mathrm{T}}^{i}(s), \tag{8}$$

and the corresponding frequency response is given by

$$\Delta\omega(s) = \frac{1}{2H_{\mathrm{sys}}} \left(\frac{1}{s^3} \sum_{i=1}^{G} \alpha_i U_{\mathrm{o}}^{i} G_{\mathrm{T}}^{i}(s) - \frac{\Delta P_{\mathrm{e}}}{s^2} \right) \tag{9}$$

where the first term represents the combined PFR of the SGs, and the second term represents the disturbance. The initial frequency decline caused by the ΔP_{e} term is arrested by the increasing PFR term, creating the frequency nadir.

To avoid the complexities of the 4th-order transfer functions $G_{\mathrm{T}}^{i}(s)$, we further assume that the turbine time constants T_4, T_5, T_6, T_7 are all small, i.e., $T_{\max} = \max\{T_4, T_5, T_6, T_7\}$ much faster than 1s. We decompose $G_{\mathrm{T}}^{i}(s)$ by approximating each $\frac{1}{s\tau+1}$ block with a second-order polynomial as

$$\frac{1}{s\tau + 1} \approx 1 - s\tau + s^2\tau^2. \tag{10}$$

The approximation accurately represents the original expression in the frequency range $\mathcal{R} = [0, \frac{1}{T_{\max}}]$. Since $G_{\mathrm{T}}^{i}(s)$ has unity DC-gain and is composed of a series of low-pass filters with cutoff frequencies $\{\frac{1}{T_4}, \frac{1}{T_5}, \frac{1}{T_6}, \frac{1}{T_7}\}$, its gain remains roughly constant in the range $\mathcal{R}$ and decreases by around $-20\mathrm{dB/dec}$ above the range. As such, the gain of the PFR term is primarily driven by $\frac{1}{s^3}$, which decreases by $-60\mathrm{dB/dec}$ at all frequencies. This causes low frequency components to have much greater gains than high frequency components (i.e. 10^{-1}rad/s has a magnitude $\sim$ 120dB greater than 10^{1}rad/s). At frequencies above the range $\mathcal{R}$, the gain is much lower than that of the dominant low frequency components, and since (10) produces approximation errors at high frequencies, the errors have low magnitudes.

By substituting (10) into $G_{\mathrm{T}}^{i}(s)$ in (9), expanding the expression, and neglecting terms higher than second-order, we find that

$$\Delta\omega(s) = \frac{1}{2H_{\mathrm{sys}}} \left(\frac{1}{s^3}(c_1 - c_2 s + c_3 s^2)) - \frac{\Delta P_{\mathrm{e}}}{s^2} \right) \tag{11}$$

where c_1, c_2, c_3 are coefficients which depend on the turbine parameters and on $\alpha_1, \ldots, \alpha_G$. Taking inverse Laplace transform of (11), the frequency nadir can be computed in closed form to be

$$\Delta\omega_{\mathrm{nadir}} = \frac{1}{2H_{\mathrm{sys}}} \left(-\frac{(c_2 + \Delta P_{\mathrm{e}})^2}{2c_1} + c_3 \right) \tag{12}$$

and imposing the bound $\Delta\omega_{\mathrm{nadir}} \geq -|\Delta\omega_{\mathrm{lim}}|$ leads to the final inequality

$$\Delta P_{\mathrm{e}} \leq \underbrace{\sqrt{4H_{\mathrm{sys}} c_1 \left|\Delta\omega_{\mathrm{lim}}\right| + 2c_1 c_3} - c_2}_{\Delta P_{\mathrm{e,max}}} \tag{13}$$

for the maximum permissible power disturbance.

IV. Iterative Restoration Sequence Computation

We now describe how the frequency nadir constraint (13) is integrated into the restoration planning problem (3). During the restoration window $\{1, \ldots, T\}$, step power imbalances $\boldsymbol{\Delta P}_{\mathrm{e}} \in \mathbb{R}^{1\times T}$ occur due to load pickup and generator cranking, which can be expressed as

$$\begin{aligned} \boldsymbol{\Delta P}_{\mathrm{e}}(k) = \boldsymbol{P}_{\mathrm{d}}^{\top} \left(\boldsymbol{b}_{\mathrm{d}}(k) - \boldsymbol{b}_{\mathrm{d}}(k-1)\right) \\ + \boldsymbol{P}_{\mathrm{c}}^{\top} \left(\boldsymbol{b}_{\mathrm{gc}}(k) - \boldsymbol{b}_{\mathrm{gc}}(k-1)\right). \end{aligned} \tag{14}$$

The parameters c_1, c_2, c_3, and H_{sys} in (13) are defined for each time step of the MILP (3), and depend on the statuses of the generators $\boldsymbol{b}_{\mathrm{g}}$. Inserting (14) as the left-hand side of (13) yields a nonlinear mixed-integer constraint, which is incompatible with the MILP. To address this limitation, we introduce a receding-horizon computation, where successive MILPs are solved with a user-defined time horizon T.

As notation, define the stacked binary status matrix $\boldsymbol{b} = \mathsf{col}(\boldsymbol{b}_{\mathrm{b}}, \boldsymbol{b}_{\mathrm{l}}, \boldsymbol{b}_{\mathrm{d}}, \boldsymbol{b}_{\mathrm{g}})$ that defines the restoration sequence, and the stacked initial values vector $\boldsymbol{b}^0 = \mathsf{col}(\boldsymbol{b}_{\mathrm{b}}^0, \boldsymbol{b}_{\mathrm{l}}^0, \boldsymbol{b}_{\mathrm{d}}^0, \boldsymbol{b}_{\mathrm{g}}^0)$. Our proposed method is shown in Algorithm 1, where terms with "$\hat{\ }$" denote predicted values of the variables.

The algorithm begins with the initial status $\boldsymbol{b}^0$ of all elements. The key idea in Steps 4–7 is to construct forward predictions

Algorithm 1 Iterative Restoration Sequence Computation

```
Initialize b^0
Initialize plan = [b^0]
while b^0 ≠ 𝟙 do
    Using plan, construct predictions b̂_gr, b̂_go ∈ {0,1}^{G×T}
    Evaluate H_sys and α in (5), (6), using b̂_gr and b̂_go
    Evaluate c_1, c_2, c_3 in (11) using H_sys and α
    Evaluate ΔP_e,max using (13)
    Solve the MILP (3),(13) for T steps
    Update initialization b^0 = b(1)
    [plan] ← [plan, b(1)]
end while
```

of the variables $\boldsymbol{b}_{\text{gr}}$ and $\boldsymbol{b}_{\text{go}}$; this can be done since ramping occurs after a fixed amount of time following activation of a generator. Based on these predictions, the right-hand side of (13) can be evaluated over a T-step horizon into the future. This renders the constraint (13), (14) *linear* in the decision variables $\boldsymbol{b}_{\text{d}}$ and $\boldsymbol{b}_{\text{gc}}$. The restoration plan is then computed for T steps. The next immediate restoration action $\boldsymbol{b}(1)$ is saved as part of the final plan, and the remaining actions computed in this iteration are discarded. The process proceeds forward recursively, and terminates once all network elements have been restored.

V. Simulation and Case Study

A. Test System

A modified IEEE 9-bus system shown in Fig. 4 is used to verify the effect of frequency constraints on the optimal restoration sequence. Parameters of the generators and their IEEEG1 turbine-governors use values referenced from [21] and [22]. Cranking time and ramp rates are chosen within the ranges reported in [23]. Loads in the system are located on buses 4-9 and split into blocks sized between 3-16 MW. Generator 1 is designated as the BSU and generators 2-3 as NBSUs. For details about the implementation and parameters, refer to [18].

B. Frequency Nadir Prediction

To verify the accuracy of the ramp approximation, frequency nadir prediction errors are shown in Fig.5 for the 9-bus system with all generators online.

For smaller imbalances, SAT1 remains inactive or saturates briefly, leading to higher prediction errors. As the imbalance increases, the corresponding change in ΔP_{ref} triggers SAT1 more consistently, resulting in lower prediction errors. Prediction accuracy is highest near the maximum imbalance permitted by the nadir constraint, though estimates remain optimistic due to the assumption of maximum generator ramping. In the 9-bus system, the smallest load—3 MW—yields a negligible nadir error on the order of 10^{-4} Hz. These results confirm that the nadir is predicted with high accuracy and that the MILP effectively enforces the frequency limit $\Delta\omega_{\text{lim}}$ in (13).

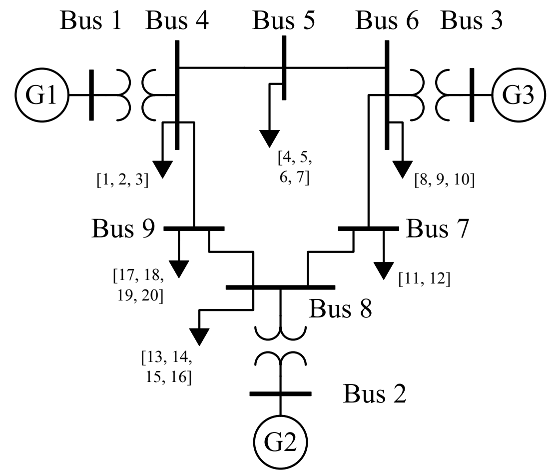

Fig. 4: Modified IEEE 9-bus system. Number in brackets denote the indices of loads on each bus

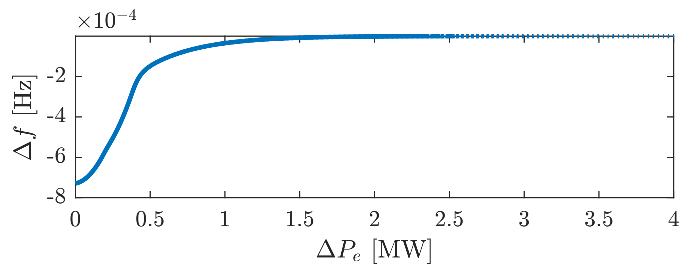

Fig. 5: Frequency nadir estimation error of the ramp approximation

C. Restoration Sequences

Two optimal restoration sequences are found by following the iterative method described in Algorithm 1. The first sequence ignores frequency constraints, while the second enforces a 1 Hz nadir limit. Fig. 6 illustrates the system's frequency when actions from the sequences are carried out every two minutes to allow transient dynamics to settle. Simulations are conducted in MATLAB using the ASF swing equation and the IEEEG1 governor-turbine model.

In the unconstrained case, all generators and loads are energized in rapid succession. Restoration completes in 40 steps as NBSUs become online, but frequency dips exceed 4 Hz, rendering the plan infeasible. Such violations risk triggering protection systems and damaging equipment.

In contrast, enforcing a 1 Hz nadir constraint results in a more gradual sequence. Early stages involve only small load pickups due to low system inertia. After each NBSU turns on, the system is able to withstand a great electrical power imbalance. With each generator start-up, the plan selects loads that would not cause any frequency violations. Although this sequence takes longer to complete, it satisfies all constraints and offers a practical and safe implementation path.

To validate the MILP-generated plan under realistic conditions, the frequency-constrained sequence is re-evaluated in PSSE. Unlike MATLAB, PSSE includes full nonlinear power

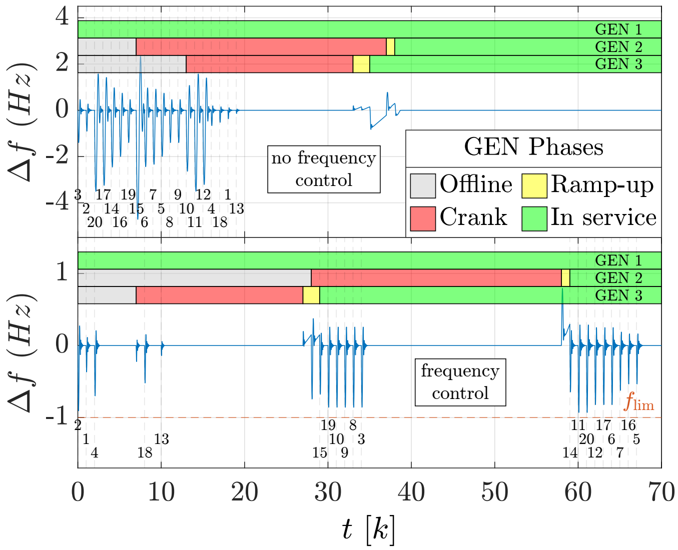

Fig. 6: Frequency behaviour during restoration sequences. Label numbers indicate the indices of restored loads

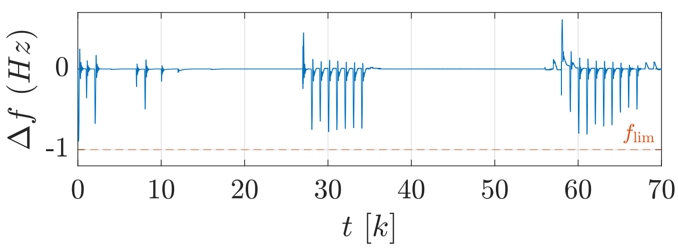

Fig. 7: PSSE Simulation of frequency-constrained restoration

flow and detailed generator dynamics. Fig. 7 shows that all restoration actions meet the frequency nadir limit of 1 Hz, with minor deviations attributable to regional governor responses. These results demonstrate that the proposed method produces frequency-constrained restoration plans that remain valid under high-fidelity dynamic simulations.

VI. Conclusion

We have provided a new approach to compute frequency-constrained optimal restoration sequences. Our approach leverages a novel approximation of the frequency nadir experienced after a restoration action is taken, along with a receding-horizon iterative computational approach to solve the resulting nadir-constrained MILP. The method is validated with a case study in both MATLAB and PSS/E, and will assist ISOs in developing fast and safe restoration plans. Future work will extend this framework to account for voltage stability, and the participation of IBRs in the restoration process.

References

[1] "Shedding light on the economic costs of long-duration power outages: A review of resilience assessment methods and strategies," *Energy Research & Social Science*, vol. 99, p. 103055, 2023.

[2] *Ontario Power System Restoration Plan*, Issue 22.0 ed., Independent Electricity System Operator (IESO), Ontario, Canada, Dec. 2024.

[3] M. Adibi, P. Clelland, L. Fink, H. Happ, R. Kafka, J. Raine, D. Scheurer, and F. Trefny, "Power system restoration - a task force report," *IEEE Trans. Power Syst.*, vol. 2, no. 2, pp. 271–277, 1987.

[4] M. M. Adibi, J. N. Borkoski, and R. J. Kafka, "Power system restoration - the second task force report," *IEEE Trans. Power Syst.*, vol. 2, no. 4, pp. 927–932, 1987.

[5] W. Jang, H. Huang, K. R. Davis, and T. J. Overbye, "Considerations in the automatic development of electric grid restoration plans," in *Proc. NAPS*, 2021, pp. 1–6.

[6] Y. Zahraoui, I. Alhamrouni, S. Mekhilef, M. R. Basir Khan, M. Seyedmahmoudian, A. Stojcevski, and B. Horan, "Energy management system in microgrids: A comprehensive review," *Sustainability*, vol. 13, no. 19, 2021.

[7] S. Poudel, A. Dubey, and K. P. Schneider, "A generalized framework for service restoration in a resilient power distribution system," *IEEE Syst. J.*, vol. 16, no. 1, pp. 252–263, 2022.

[8] F. Qiu, Y. Zhang, R. Yao, and P. Du, "Power system restoration with renewable participation," *IEEE Trans. Sust. Energy*, vol. 14, no. 2, pp. 1112–1121, 2023.

[9] H. Huang, P. Ju, Y. Jin, X. Yuan, C. Qin, X. Pan, and X. Zang, "Generic system frequency response model for power grids with different generations," *IEEE Access*, vol. 8, pp. 14 314–14 321, 2020.

[10] M. Gholami, J. Moshtagh, and N. Ghadernejad, "Service restoration in distribution networks using combination of two heuristic methods considering load shedding," *J. mod. power syst. clean energy*, vol. 3, no. 4, pp. 556–564, 2015.

[11] N. Rhodes, C. Coffrin, and L. Roald, "Recursive restoration refinement: A fast heuristic for near-optimal restoration prioritization in power systems," *Electric Power Systems Research*, vol. 212, p. 108454, 2022. [Online]. Available: https://www.sciencedirect.com/science/article/pii/S0378779622005934

[12] J. M. Miller, H. N. Villegas Pico, I. Dobson, A. Bernstein, and B. Cui, "Feedback control approaches for restoration of power grids from blackouts," *Electric Power Syst. Research*, vol. 211, p. 108414, 2022.

[13] H. Hijazi, T. W. Mak, and P. Van Hentenryck, "Power system restoration with transient stability," *AAAI*, vol. 29, no. 1, Feb. 2015. [Online]. Available: https://ojs.aaai.org/index.php/AAAI/article/view/9241

[14] L. Liu, W. Li, Y. Ba, J. Shen, C. Jin, and K. Wen, "An analytical model for frequency nadir prediction following a major disturbance," *IEEE Trans. Power Syst.*, vol. 35, no. 4, pp. 2527–2536, 2020.

[15] F. Bullo, *Lectures on Network Systems*. CreateSpace Independent Publishing Platform, 2018. [Online]. Available: https://books.google.ca/books?id=JpoxtwEACAAJ

[16] J. Glover, T. Overbye, and M. Sarma, *Power System Analysis and Design*. Cengage Learning, 2016. [Online]. Available: https://books.google.ca/books?id=KHYcCgAAQBAJ

[17] F. Qiu and P. Li, "An integrated approach for power system restoration planning," *Proc. IEEE*, vol. 105, no. 7, pp. 1234–1252, 2017.

[18] I. Farhat and X. Y. Zou, "BSPSSEPy application v0.4." [Online]. Available: https://github.com/aldahabi27/BSPSSEPy

[19] M. L. Chan, R. D. Dunlop, and F. Schweppe, "Dynamic equivalents for average system frequency behavior following major distribances," *IEEE Trans. Power Apparatus & Syst.*, vol. PAS-91, no. 4, pp. 1637–1642, 1972.

[20] I. C. Report, "Dynamic models for steam and hydro turbines in power system studies," *IEEE Trans. Power Apparatus & Syst.*, vol. PAS-92, no. 6, pp. 1904–1915, 1973.

[21] P. Anderson, A. Fouad, and Institute of Electrical and Electronics Engineers, *Power System Control and Stability*, ser. IEEE Press power engineering series Power system control and stability. Wiley, 2003.

[22] Neplan AG, "Turbine-governor models: Standard dynamic turbine-governor systems in neplan power system analysis tool," *Tech. Rep.*, 2015.

[23] A. B. Birchfield, "Graph decomposition for constructing blackstart restoration strategies in benchmark cases," *Electric Power Syst. Research*, vol. 212, p. 108402, 2022. [Online]. Available: https://www.sciencedirect.com/science/article/pii/S0378779622005533